

Effectiveness of Stent in the Treatment of Renal Artery Aneurysm using FSI Simulation

H. Abu Bakar, A. Abas[†] and N. Razak

School of Mechanical Engineering, Universiti Sains Malaysia, Engineering Campus, 14300 Nibong Tebal, Pulau Pinang, Malaysia

[†]Corresponding Author Email: aizatabas@usm.my

(Received October 7, 2018; accepted December 3, 2018)

ABSTRACT

Renal artery aneurysm (RAA) is a condition that affects approximately 0.1% of the general population. The rate of incidence is minimal compared to other type of aneurysm but a high number of ruptures have been reported in pregnancy, especially at the third trimester. The concerning issue is that the maternal mortality rate stretches up to 50% and the fetal mortality rate approaching 85% with a universal loss of the affected kidney. This study aimed at investigating the effectiveness of stent in treatment of RAA using the fluid-structure interaction (FSI) approach. The flow pattern, wall shear stress (WSS), deformation and von Mises stress experienced are compared between RAA model without stent and with Abbott RX Herculink stent. A simple PIV experiment, observing the flow profile was conducted as a validation steps in ensuring the simulation results are reliable and accurate. The findings show that the simulation and PIV data are in good agreement in terms of the flow profile. The presence of stent managed to reduce the blood flow maximum velocity down to 46% and minimized the circulation of blood in the aneurysm dome. As for the WSS, the used of stent succeeded in decreasing the WSS experienced by the wall of aneurysm by 71% and below the baseline level of WSS that could induced rupture. The deformation of RAA and maximum von Mises stress reduced by 58% and 73% respectively when stent is used. In addition, the maximum von Mises stress after the stent placement is lower than the threshold value for the ultimate tensile strength of the tissue. This study concluded that the stent placement is effective in reducing the risk of aneurysm rupture in renal artery it can be one of the baseline for the further study regarding the RAA.

Keywords: Renal artery aneurysm; Stent; FSI; PIV.

NOMENCLATURE

p	pressure	v	velocity
Δt	time interval		
Δx	fluid displacement	ρ	density

1. INTRODUCTION

Aneurysm is an arterial condition that occurs because of the weakening of the blood vessel wall (Mokhtar *et al.* 2017). In time, the weak wall stretched and formed an irreversible bulge, which if not treated, increased the risk of rupture and haemorrhage (Alagheband *et al.* 2015). Renal artery aneurysm (RAA) commonly happens in the shape of a berry-like known as saccular (Eskandari & Resnick, 2005). The probability of it to happen is approximately 0.1% of the general population (Coleman & Stanley, 2015; Tsilimparis *et al.*, 2013). This preliminary assumption is based on the autopsy results, and with the recent technology in

the angiography, the true incidence is expected to be higher (Hwang *et al.* 2011). The natural history of RAA is barely known and its symptoms are non-existent (Barros *et al.*, 2014). Fibrodysplasia, congenital disorder, trauma and inflammatory causes are a few suggested etiology of the RAA (Malacrida *et al.* 2007). The complications associated with RAA includes the renovascular hypertension, renal artery thrombosis and rupture which could lead to death (Eskandari & Resnick, 2005). Even though the estimated incidence of RAA cases is very minimal, a high number of ruptures have been reported in pregnancy, especially at the third trimester. The concerning issue is that the maternal mortality rate stretches up

to 50% and the fetal mortality rate approaching 85% with a universal loss of the affected kidney (Maughan *et al.* 2015).

The treatment for RAA can be of two types; a conventional surgery and an endovascular procedure. The advancement of the latter has reduced the morbidity and mortality rate, with the advantage of preserving the native vascular tree (Barros *et al.*, 2014). Endovascular (EVAR) is a novel minimally invasive technique performed as an alternative to conservative surgical method and it is included in the management options for the elective repair of the arterial aneurysm (Mokhtar *et al.*, 2017). Among the advantages of EVAR are reduced post-operative complications and shortened length of stay in the hospital in comparison with open surgery treatments (Tsilimparis *et al.*, 2013). Wang *et al.* (2018) stated that EVAR is one of the most definitive method for treating RAA due to the capability of the technique to isolate aneurysm from the main bloodstream while at the same time managed to keep the artery fluent and unobstructed.

For the EVAR treatments, two popular techniques are the coil embolization and stent-graft placement. The preference of stent-graft are due to a likelihood of delayed recanalization of the aneurysm and the migration of the coils embolization technique (Sahin *et al.* 2007). On the other hand, stent-graft offered a complete sealing of the neck of aneurysm (Sahin *et al.*, 2007). Chandra *et al.* (2014) reported a successful exclusion of two large saccular-shaped aneurysms, nearby RAA located in the proximal renal artery. The placement of Viabahn covered stent managed to exclude the RAA. This is supported by a 2-year follow-up of the patient which shows no requirement of post-operative procedure and the RAA remained asymptomatic. Muzaffer Degertekin *et al.* (2006) treated a 54-year old woman with saccular-shaped aneurysm situated just at the mid-portion of the right renal artery using balloon-expandable Jostent GraftMaster stent (Abbott Vascular Instruments) and after 6-month of follow-up, the exclusion aneurysm was achieved. Sahin *et al.* (2007) in their case study, treated a wide-necked left RAA with stenosis by means of balloon-expandable stent-graft (Jostent Stent Graft, Abbott Vascular). Sousa and Mansilha (2017) also opted for self-expandable open-cell nitinol stent (Evert, Abbott Vascular) to treat a 21 mm saccular aneurysm in the artery's trifurcation and proximal inferior segmental artery. A complete angiography afterwards demonstrated a total segregation of the aneurysm with the preservation of the renal perfusion.

This study intends to investigate the effectiveness of the stent technique in treating RAA. The lack of exploration in the RAA in comparison with other aneurysms may due to the low incidence rate of the RAA itself. However, the authors believed in the importance of examining the RAA as much as other aneurysm because of the disastrous consequences especially to pregnant patients that could happen if the aneurysm ruptured. The stent that will be used in this study is based on Abbott

RX Herculink stent that is specifically designed for the renal artery. According to Chrysant *et al.* (2014), 74.3% of the patients that had EVAR of Abbott RX Herculink stent had a reduction in systolic blood pressure and freedom of major adverse events up to 98.5% after 30-days. To investigate the effectiveness of the stent to treat RAA, fluid-structure interaction (FSI) simulations of the blood flowed through the RAA is conducted and parameters such as velocity and wall shear stress (WSS) are compared between the cases of with and without stent placement in the renal artery. Avrahami *et al.* (2012) investigated the flow and stress field of a fenestrated endograft structures with FSI technique to observe the potential risk of endograft detachment or fracture. Drewe *et al.* (2017) performed FSI simulations on the models of Abdominal Aortic Aneurysm (AAA) to study the effects of proximal neck and iliac bifurcation angle on AAA wall stress and hemodynamic. Javadzadegan *et al.* (2014) also performed FSI simulations to examine the influence of spiral flow on the hemodynamic changes in the elastic AAA model. Even though FSI has been widely used in the aneurysm studies, the study is focusing more on the abdominal aortic and intracranial aneurysm rather than RAA (Javadzadegan *et al.*, 2014; Jayendiran *et al.* 2018; Khe *et al.*, 2016; Lin *et al.* 2017; Rissland *et al.* 2009; Valencia *et al.*, 2013; Wang & Li, 2011). This may be due to the fact that the incidence rate of RAA is lower compared to other aneurysm conditions. In addition, growth rate of RAA is not as rapid as other aneurysm conditions, which is around 0.86 mm/year (Klausner *et al.* 2015).

Despite that, a separate study on RAA is crucial because the aetiology of RAA is different from other aneurysm conditions. Furthermore, the intervention for RAA is also different from others due to different size and location of the lesion. Most of the studies regarding RAA have been from the case reports (Canyigit M, Cam A, Cetin H, Altunoğlu A, & M., 2015; Chandra *et al.*, 2014; Maughan, Webster, Konig, & Renfrew, 2015a; Sousa & Mansilha, 2017) and the study of RAA from numerical simulation perspective is very limited. Hence, the authors believed that a thorough study is required as a baseline study for RAA similar to other aneurysm conditions. Moreover, the effectiveness of stent in reducing the risk of RAA rupture is also discussed.

2. METHODOLOGY

2.1 Fluid-Structure Interaction

Fluid-structure interaction (FSI) is a branch of computational fluid dynamic (CFD), where it shows the interaction between the fluid dynamics law and structural mechanics. In this study, FSI setup will be employed to study the effect of blood flow inside renal artery with saccular aneurysm condition. The coupling of ANSYS transient structural and Fluent using 'system coupling' will produce the results with the interaction between the aneurysm structure and the blood flow.

In the ANSYS Fluent, the computation of the governing equations will happen until it reached a convergence solution. The solution will provide the forces required for the structural part in the ANSYS Structural. This transferring of information is done through the ‘system coupling’ system in the ANSYS software. The deformation caused due to the forces will be transferred back to the Fluent. This process repeats until both parts achieved the convergence condition set. Figure 1 exhibit the process of ANSYS FSI computation.

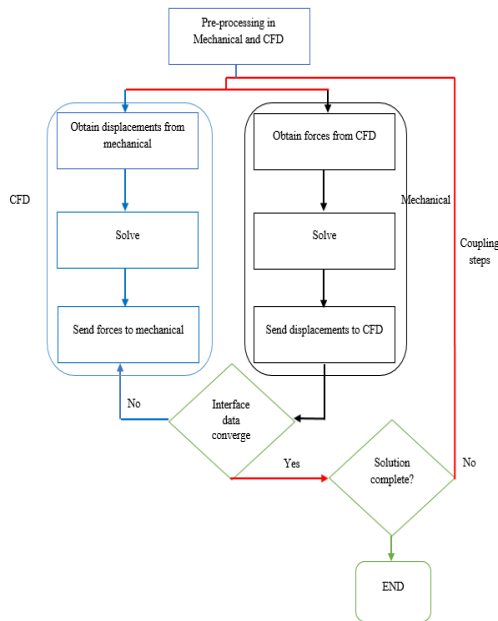


Fig. 1. ANSYS FSI computation process diagram.

2.1.1 Governing Equations

The governing equations related are the continuity equation and the Navier-Stokes equation for the fluid part.

Continuity equation

$$\frac{\partial \rho}{\partial t} + \nabla \cdot (\rho \mathbf{v}) = 0 \quad (1)$$

Navier-Stokes equation

$$\rho \left(\frac{d\mathbf{v}}{dt} + \mathbf{v} \cdot \nabla \mathbf{v} \right) = -\nabla p + \mu \nabla^2 \mathbf{v} + \mathbf{f} \quad (2)$$

The ρ represents the blood’s density, \mathbf{v} is the blood’s velocity, and p is the blood’s pressure. Blood is a non-Newtonian fluid, which means that the blood does not have constant viscosity. The blood has shear thinning like behavior where it becomes less viscous with an increase in stresses applied to it. However, [Suess *et al.* \(2016\)](#) explained that the effect of non-Newtonian characteristic of the blood is only applicable in vessel with diameter of less than 1 mm. Therefore, for this study, the authors simply considered the blood as a Newtonian fluid with density of 1050 kg/m³ and dynamic viscosity of 0.0035 Pa.s.

2.2 Boundary Conditions (BC)

2.2.1 Structural Model

For the structural part, the artery with aneurysm and stent, BC is set in the ANSYS Structural setup. Both end faces of the artery are set to be fixed support, and the interior of the artery is set as ‘Fluid-structure interface’. The interior of the artery are selected according to the surfaces that will be in contact with the fluid domain. Fig. 2(a) shows the BC for structural model.

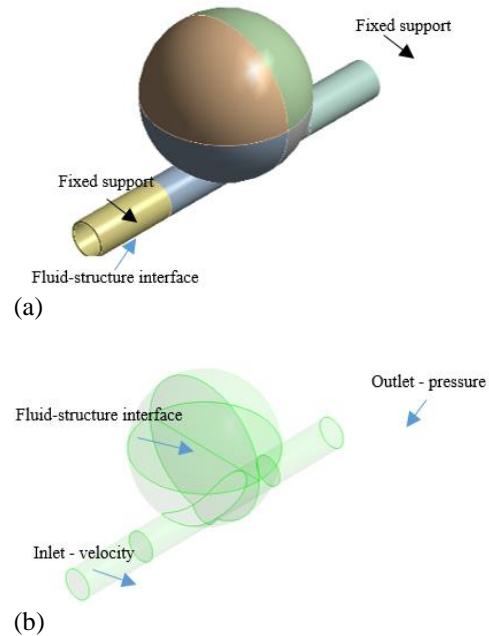


Fig. 2. (a) Boundary conditions for structural model; (b) Boundary conditions for fluid model.

2.2.2 Fluid Model

For the fluid domain (blood) the BCs are set in the ANSYS Fluent setup. The blood flow operates in a pulsatile and cyclic state. For this reason, the velocity of the blood will be in the time varying periodic profile. The combination of systolic, the period where the heart contracted and pumps the blood, and diastolic, the period where the heart rest between the two beats, created a pulsatile profile for the blood flow. The pulsatile flow formulation in this study is based on [Sinnott *et al.* \(2006\)](#). A normal heart beat of an adult (60 bpm) with a peak velocity of 0.5 m/s and minimum velocity of 0.1 m/s is implied in the formulation. The systolic pressure is 90 mmHg and diastolic pressure is 45 mmHg for a normal human in the renal artery ([Myer, 2003](#)). Hence, for simplicity, the average of both phases which is 67.5 mmHg (9,000 Pa) will be used as the static gauge pressure at the outlet. The surface of the blood region (except for the inlet and outlet) are selected as ‘Fluid-structure interface’. The ‘System coupling’ system will detect these fluid-structure interfaces for the transferring of forces and displacements data. Figure 2(b) shows the summary of BCs for the fluid model.

2.3 CAD Model

2.3.1 Renal Artery Aneurysm

The renal artery model is an idealized model with the size of the aneurysm taken from one of the study cases reported by [Bracale *et al.* \(2017\)](#). The size of the aneurysm is 28×24 mm. The diameter of renal artery is 6 mm ([Bracale *et al.*, 2017](#); [Suess *et al.*, 2016](#)), the thickness is 0.5 mm ([Leertouwer *et al.*, 1999](#)) with the length of 65 mm. In this study, the renal artery material properties are taken as isotropic, linear elastic solid [Corey J. Drewe *et al.* \(2017\)](#) with density of 2000 kg/m^3 , Young modulus of 2.7 MPa and Poisson ratio of 0.45. Figure 3 is the 3D model of the representation of RAA and Table 1 summarized the dimensions and material properties.

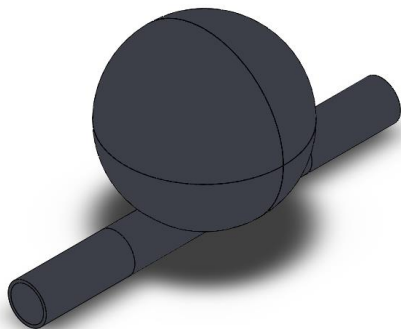


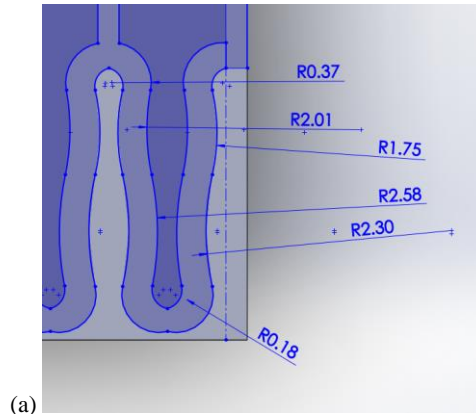
Fig. 3. CAD model of renal artery with aneurysm.

Table 1 Summary of dimensions and material properties of RAA

Dimensions and material properties of RAA	
Diameter of renal artery	6 mm
Length of the renal artery	65 mm
Thickness of renal artery	0.5 mm
Size of the aneurysm	28×24 mm
Density	2000 kg/m^3
Young modulus	2.7 MPa
Poisson ratio	0.45

2.3.2 Stent

The stent design for this study is based on Abbott RX Herculink for renal artery. According to [Chrysant *et al.* \(2014\)](#), 74.3% of the patients that had EVAR using this type of stent had a reduction in systolic blood pressure after 3 years. [Chrysant *et al.* \(2014\)](#) also claimed that the stent provided freedom from major adverse events up to 98.5% at 30 days and the mean baseline systolic blood pressure significantly decreased post procedure and through 36 months. However, the only dimensions available through public search are the diameter and length of the stent. Therefore, the approximation dimensions is based on the renal artery model that is constructed and shown in Fig. 4.



(a)



(b)

Fig. 4. (a) Stent's dimensions; (b) Final design of the 3D model of the stent based on Abbott RX Herculink.

2.4 Meshing Process

Mesh is an important aspect in the simulation process as it can affect the accuracy and computational time required to complete the simulation. In this study, hexagonal-shaped element is the preferable shape because it can reduce the overall count of element and shorten the computational time compared to the tetrahedral-shaped element. In addition, the tetrahedral element is easily distorted and this can result in the divergence state in computation process. For the structural and fluid models, an element size of 7.10×10^{-4} m is used with total number of elements of 12,383 and 67,107 respectively. This choice of element size is based on the mesh convergence analysis explained further in this research. Figure 5 shows the meshing done to the structural and fluid models.

2.5 Mesh Convergence Analysis

The objective of performing the mesh convergence analysis is to obtain the optimum and suitable mesh size and number of elements for the simulation process. The size of the mesh will affect the results accuracy and the computational time taken for the computation to complete. The smaller the size of the mesh, the more accurate the results will be but at the expense of higher cost of computational time. However, if the size of the mesh is increased, the computational time will decrease but the results will be less reliable. Therefore, finding the balanced between the solution accuracy and computational time is crucial in the simulation process.

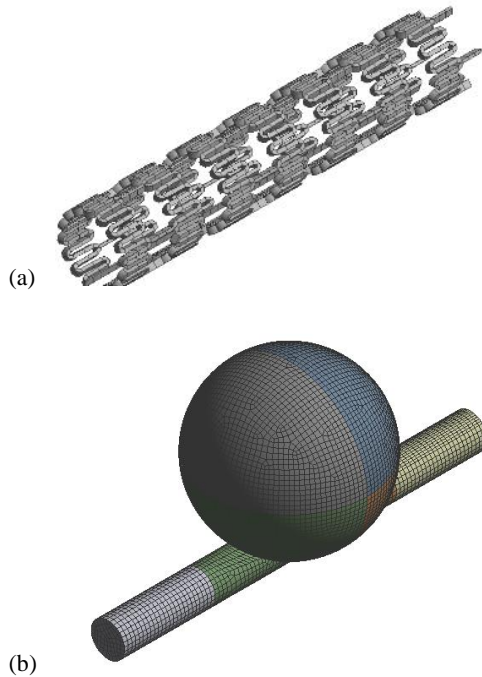


Fig. 5. (a) Meshing of renal artery aneurysm; (b) Meshing of stent; (c) Meshing of blood.

The meshing process is done through ANSYS Fluent for the fluid body. The mesh size will be changed from coarse to fine mesh size and the result of the maximum velocity of the blood flow are taken for comparison on the percentage difference between two consecutive mesh sizes. If percentage difference reaches less than 1%, it is assumed that solution accuracy is achieved and the mesh size will be chosen as the optimized mesh size for the subsequent simulations. Table 2 displays the mesh sizes and maximum velocity obtained while Fig. 6 shows the convergence of velocity as the mesh size decreased. Therefore, for this study, mesh size of 7.10-m will be used for the simulation process. Figure 6 shows the convergence of mesh size.

Table 2 Mesh convergence analysis data

Mesh size (m)	Fluid		
	Num. of elements	Maximum velocity (m/s)	Percentage difference (%)
1.10-2	11,207	0.4521	-
1.10-3	24,391	0.5817	14.93
7.10-4	67,107	0.6041	2.57
5.10-4	156,930	0.6052	0.85
3.10-4	215,348	0.6063	0.74

2.6 Particle Image Velocimetry Experiment (PIV)

Particle image velocimetry (PIV) is an optical

method commonly used in flow study. From the motion and changes in position of small tracer particles, inserted in the working fluid, the flow velocity field can be obtained (Chong Ng *et al.*, 2018). The method of computing the movement of the particle between two light pulses is given by:

$$V = \frac{\Delta x}{\Delta t} \tag{3}$$

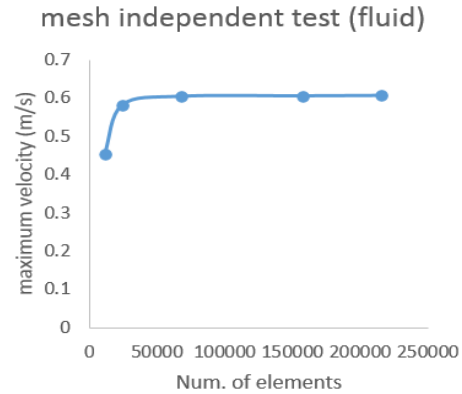


Fig. 6. Convergence graph of number of elements against maximum velocity.

where Δx is the fluid displacement and Δt is the time interval. A pulsed LED light will illuminate the tracer particles and a camera will be used to capture images of the target area. PIV experiment data will be the validation required by computational simulation and to support the visualization of flow by the computational model. A simple comparison of flow pattern between the simulation and PIV experiment results are sufficient to validate the capability of simulation process in producing the exact hemodynamic condition as in real case. The working fluid used in this experiment is known as aqueous glycerol solution. It is a mixture of 22% of glycerol by mass with water. The reason for using this working fluid is to mimic the behaviour of the blood. The density and viscosity of the solution is 1059 kg/m³ and 1.562.10-6 m²/s. The tracer particle or seeding particle used in this experiment is PSP-50; Polyamide seeding particles from Dantec Dynamics, with a diameter of 50 μm . The laser model is NANO L135-15 PIV with pulse duration of 4 ns. The camera is from Dantec HiSense MKII C8484-52-05CP Hamamatsu Digital Camera C8484-05CP with frame rate of 12.2 fps at full resolution. The time interval between images, Δt is 163 ms with 24 frames, which is 12 images to be captured for each image acquisition process.

The procedure of the experiment start with pumping the aqueous glycerol solution to the RAA model. A valve and flow meter are connected to Arduino Uno R3 board to create the pulsatile flow and to monitor the instantaneous flow rate entering the RAA model. When the fluid has filled the model completely, the LED light is activated to illuminate the seeding particles so the camera would be able to capture the flow pattern clearly. The images captured is analysed using PIVlab, a PIV tool in the Matlab software.

Figure 7 table shows the setup diagram and flow of the PIV experiment.

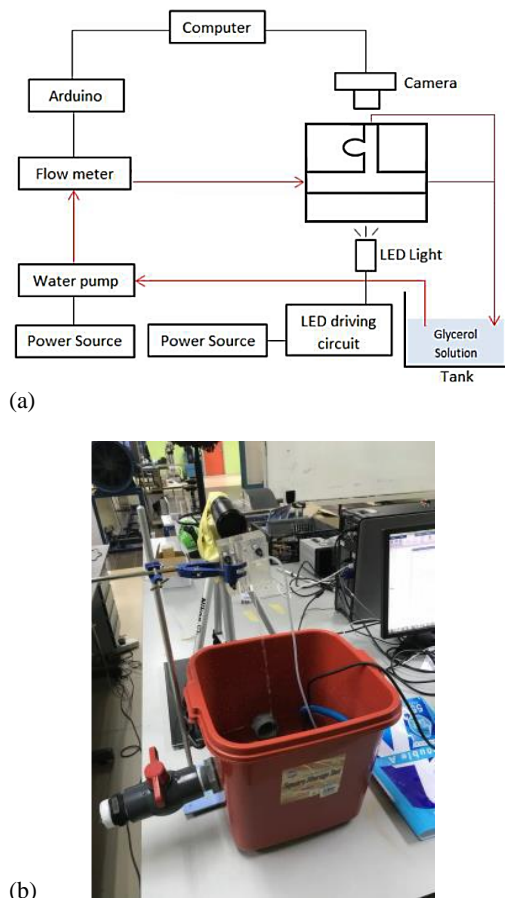


Fig. 7. (a) Flow diagram of PIV experiment; (b) experiment setup of the PIV.

3. RESULTS AND DISCUSSIONS

In this research, the objective is to study the effectiveness of stent to treat renal artery aneurysm (RAA). The velocity of the blood, wall shear stress (WSS), maximum pressure of the blood, deformation of the artery and von Mises stress are the parameters that are monitored and compared between the cases of RAA with and without stent.

3.1 PIV Validation

PIV experiment is conducted as a validation process for the simulation computed in this study. The similarity in the flow pattern between the simulation and PIV experiment data means that the simulation results are reliable and capable of producing real flow pattern.

Figure 8 compares the simulation and PIV experiment velocity vectors. According to the results, the flow pattern of the fluid in simulation and PIV appears to be the alike, with both illustration of flow vectors indicating that the fluid is circulating inside the aneurysm dome. For that reason, the simulation result is in good agreement with the PIV

data in term of the flow profile. Thus, this shows that the simulation results is capable of producing a reliable and accurate flow pattern.

3.2 Flow Pattern

The hemodynamic of the blood plays an important role in the growth and rupture of the aneurysm. The flow of the blood could induced unnecessary stress that in time will results in the expansion of the aneurysm.

The maximum velocity for time 0.1 s, 0.4 s and 0.8 s are tabulated in Fig. 9. For the case of RAA without stent, the maximum velocity is obtained at time 0.4 s (systolic period), which is 0.155 m/s and located inside the aneurysm dome. The blood is also seen entering and circulating inside the aneurysm dome. This condition is alarming because the circulation of blood could lead to the rupture of the aneurysm. Yeow and Leo (2016) stated that the ruptured aneurysm occurred in the region of blood recirculation. This may be true as Antonov *et al.* (2018) findings that the hemodynamic of the blood inside the aneurysm will deteriorate the wall strength and results in decreasing the pressure threshold and increasing the vulnerability to higher tensile forces.

For the case of RAA with stent, the maximum velocity recorded in the aneurysm dome is around 0.0825 m/s at time 0.4 s. The difference of maximum velocity between both cases is 46%. This is due to the placement of stent at the entrance of the aneurysm dome which prevents the blood from circulating inside it. In addition, the circulation of the blood inside the aneurysm is seen to be less vigorous when the stent is present in the RAA model. Yeow and Leo (2016) affirmed that eliminating irregular circulation inside the aneurysm will promote an environment suitable for the thrombus formation. Hence, based on the findings, the presence of stent could have an impact in normalizing the flow pattern and reducing the risk of aneurysm rupture due to irregular hemodynamics of the blood.

3.3 Wall Shear Stress (WSS) of the Aneurysm

Figure 10 shows the data tabulated for the WSS with and without stent implanted. As the time progresses from 0.1 s to 0.4 s, WSS also increases due to the increased in velocity inside the aneurysm dome. Afterwards, from 0.4 s to 0.8 s, WSS decreased in value due to the declining velocity value. The maximum of WSS recorded is during the peak systolic period, which is at time 0.4 s for both cases. The WSS for RAA without stent is recorded to 3.5 Pa and WSS for RAA with stent is 1.025 Pa. Therefore, it should be noted that the stent managed to reduce the maximum WSS by 71%, which is a significant reduction.

As stated earlier, WSS occurrence occurs due to the complex flow pattern that happened inside the aneurysm. Over time, this excessive blood circulation could lead to pressure built up and subsequently aneurysm rupture. On the other hand,

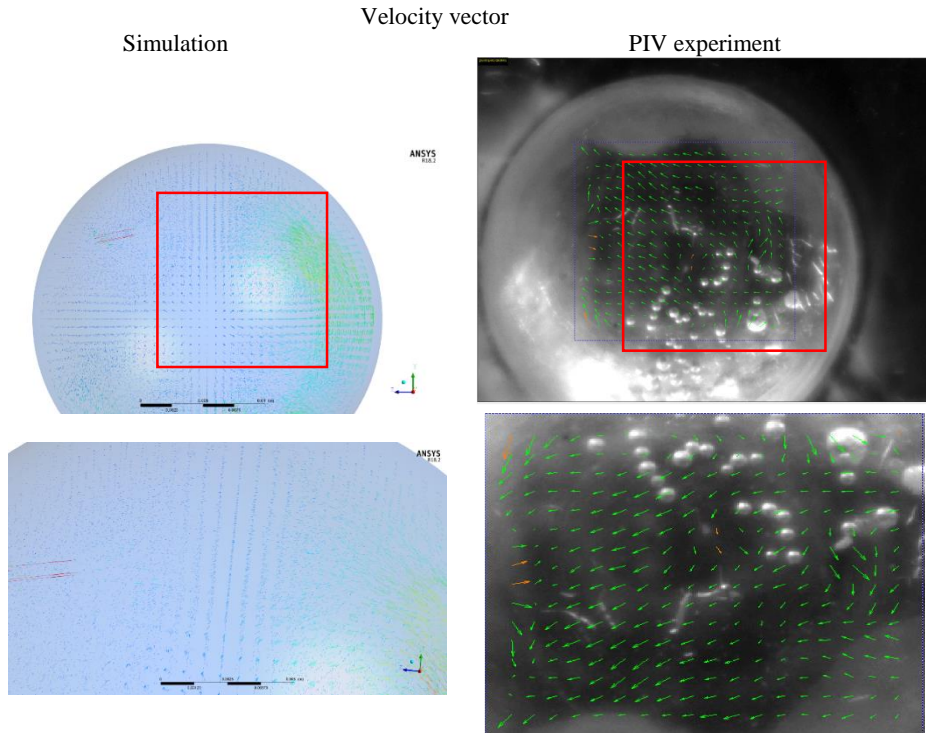


Fig. 8. Velocity vector pattern based on simulation and PIV experiment.

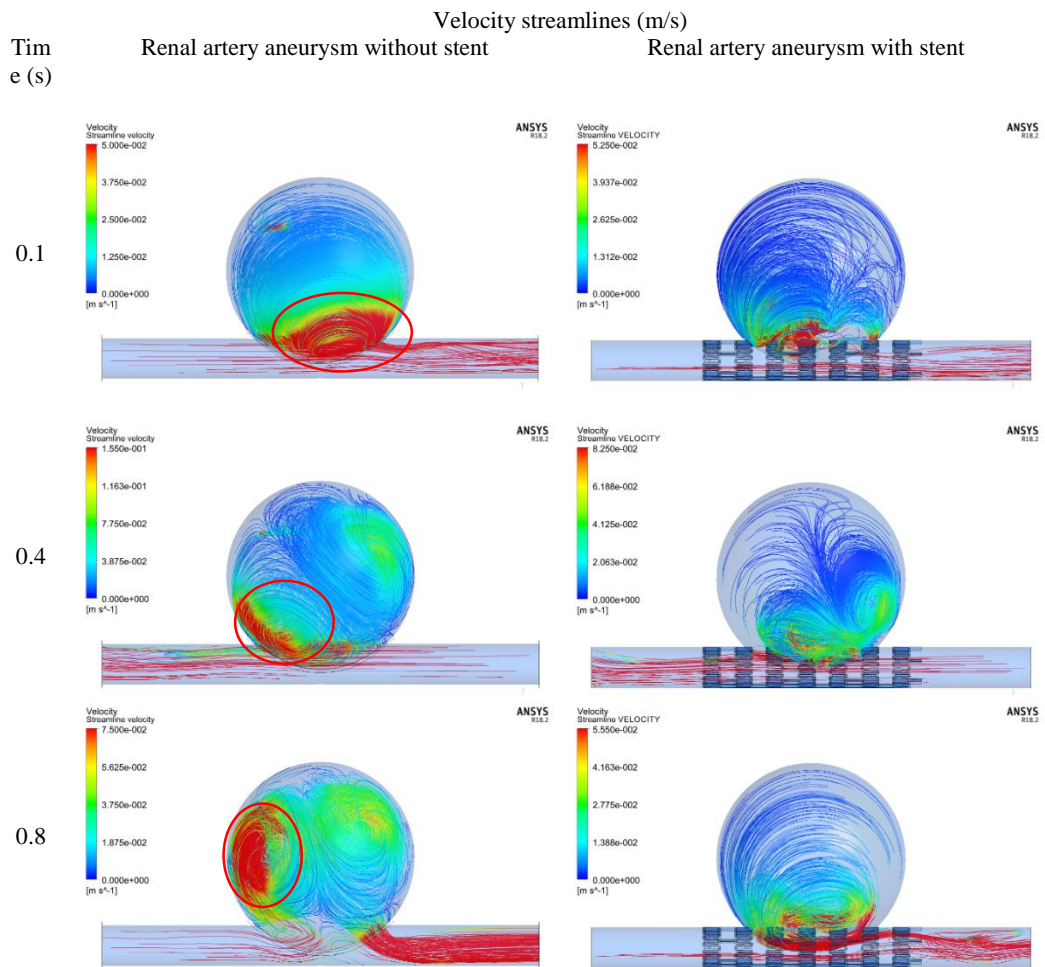


Fig. 9. Velocity streamline for cases of RAA with and without stent.

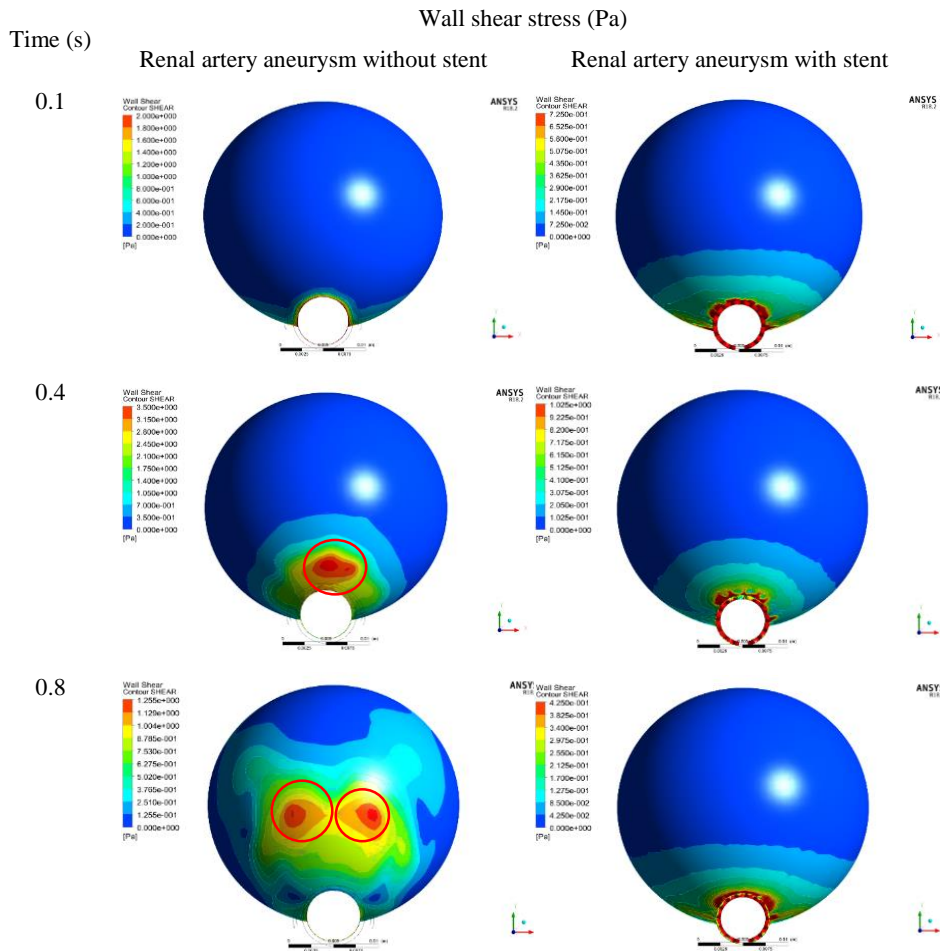


Fig. 10. Wall shear stress (WSS) for cases of RAA with and without stent.

with the presence of the stent, the flow of the blood seems to be blocked from entering the aneurysm dome. Mulder *et al.* (2009) stated that the presence of vortex, even if small-scale in size can alter the oscillating wall shear stress. Consequently, it can lead to high risk of rupture due to the disrupted flow pattern. Varble *et al.* (2017) in their studies, found that the ruptured aneurysm had nearly 1.5 times vortex structures near the surface as compared to the unruptured aneurysm. High WSS could prompt matrix metalloproteinase production through smooth muscle cells that will result in internal elastic lamina damage and cell apoptosis (Varble *et al.* 2017). Du and Lü (2017) in their study regarding the growth and rupture of saccular aneurysm mentioned that WSS of around 1.5 Pa is sufficient to induce the degeneration of endothelial cells in the aneurysm wall causing formation of lesion and subsequently could lead to rupture. (Yiemeng Hoi *et al.*, 2004) set the baseline level for WSS to be between 15 – 20 dynes/cm² (1.5 – 2.0 Pa). Hence, the simulation results shows that the presence of stent is likely to help avoid the potential for aneurysm of rupture by decreasing the WSS up to 71%, which is less than the threshold mentioned by Du and Lü (2017).

3.4 Deformation of the Renal Artery Aneurysm

Figure 11 displays the deformation that the RAA model experienced with and without the presence of stent placed at the entrance of the aneurysm dome. The distribution of deformation for both cases is different due to the presence of stent that provides a strong support to the elastic artery. At time 0.1 s, the maximum deformation for RAA without stent is 1.273.10⁻³ m. Then, at time 0.4 s of the peak systolic period, the maximum deformation decreased to 1.158.10⁻³ m. Afterwards, as it reaches the time of 0.8 s, the maximum deformation increased to 1.239.10⁻³ m. The location that experienced the maximum deformation also changed from the peak and bottom of the aneurysm dome to only the bottom section of the aneurysm dome. This happened because of the flow of the blood that continuously passing through and circulating inside the aneurysm dome. The high intensity velocity circulation profile exerts forces to the wall of the aneurysm causing it to deform as shown in Fig. 11. These results are in close agreement with Lin *et al.* (2017) in which the increased diameter of the aneurysm is caused by the continuous exertion of forces to the aneurysm wall.

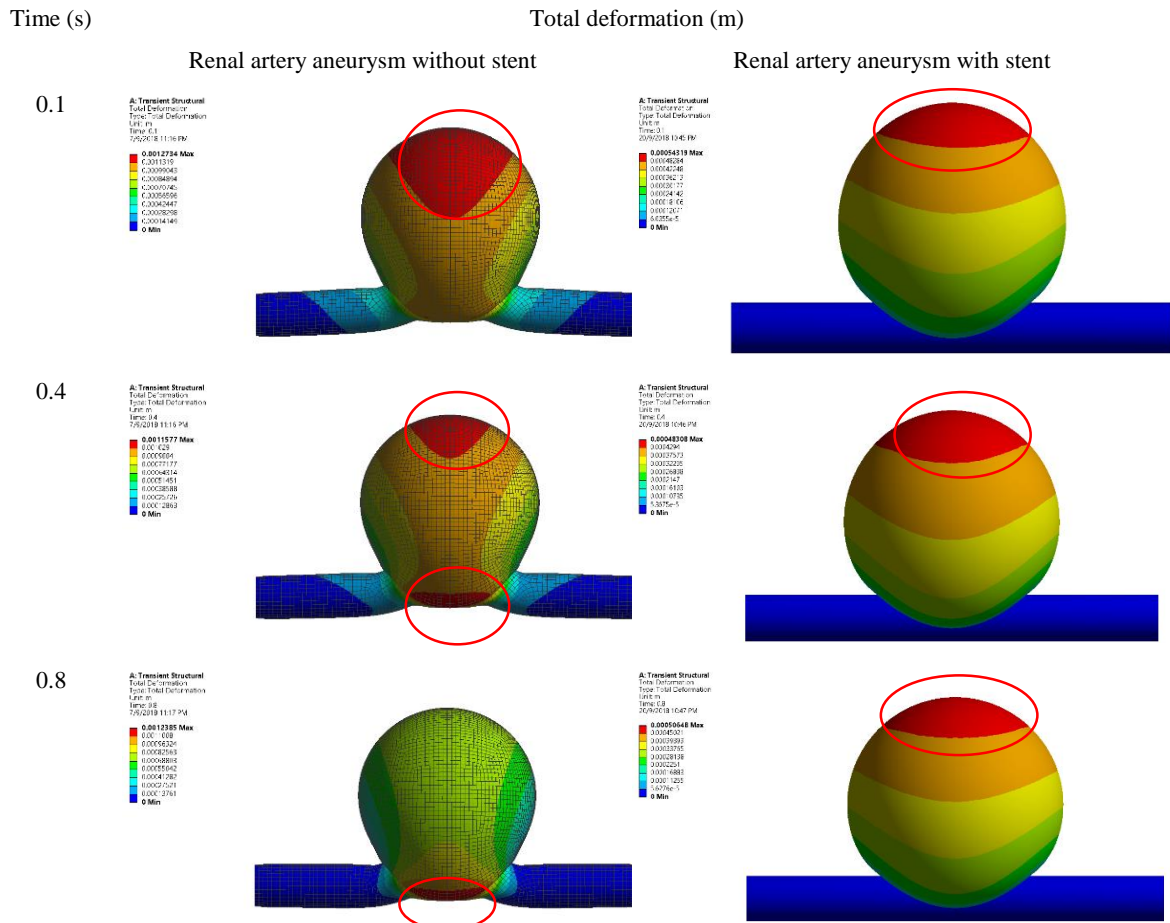


Fig. 11. Total deformation for cases of RAA with and without stent.

For the case of RAA with stent, at time 0.1 s, the maximum deformation obtained is $5.432 \cdot 10^{-4}$ m. As the time progresses to 0.4 s, the maximum deformation decreased to $4.831 \cdot 10^{-4}$ m. Finally, as the time reaches 0.8 s, the maximum deformation increased back to $5.065 \cdot 10^{-4}$ m. The distribution of deformation seems to be persistent from 0.1 s to 0.8 s, where the maximum deformation is at the peak of the aneurysm wall. The presence of the stent affected the deformation of the RAA as shown side-by-side in Fig. 11. The strong support provided by the stent prevents the renal artery from buckling. In the case of RAA without stent, the initial straight vessel became curved upwards as the blood flowed and circulated inside the aneurysm. This condition is in agreement with Sharzehee *et al.* (2018) findings as the aneurysmal artery displayed a buckling behaviour in their detailed study for the steady-state and pulsatile blood flow. The stent managed to reduce the deformation of the RAA down to 58%.

3.5 Von Mises Stress

The analysis for the von Mises stress for the cases of RAA with and without stent are tabulated in Fig. 12. The magnitude of von Mises stresses varied with time but the distribution of the stresses are quite similar throughout the simulation period. One of the theory in predicting the rupture of the aneurysm is through the ultimate strength of the tissue in which if the stresses projected to the wall of the aneurysm exceeds the threshold limit, the aneurysmal sac could

rupture Azar *et al.* (2018).

For the case of RAA without stent, the von Mises stress at 0.1 s is around 0.7921 MPa. As the time proceeds, the von Mises stress decreased to 0.7773 MPa at time 0.4 s and increased slightly up to 0.7818 MPa. On the other hand, for the case of RAA with stent, the maximum von Mises stress obtained is around 0.2182 MPa at time 0.1 s. At time 0.4 s, the maximum von Mises stress exerted to RAA is 0.2048 MPa which is a slight reduction as compared to the initial value. Finally, at time 0.8 s, the maximum von Mises stress increased back similar to the RAA without stent to 0.207 MPa.

There are many threshold limits established by other researchers regarding the maximum stress the artery could withstand before rupture. Azar *et al.* (2018) regarded stress 1 MPa is the ultimate tissue strength and exceeding it could result in aneurysm rupture. On the contrary, Giannoglou *et al.* (2006) set the threshold of the stress limit to not exceed 0.65 MPa that is almost half the value stated by Azar *et al.* (2018). Di Martino *et al.* (2006) in their study, found out that the ruptured tissue of the aneurysm had a tensile strength of 0.54 MPa. Hence, to not overestimate the condition, in this study, the threshold stated by Di Martino *et al.* (2006) will be the referred threshold for the ultimate tissue strength.

Based on Fig. 12, the von Mises stress suffered by

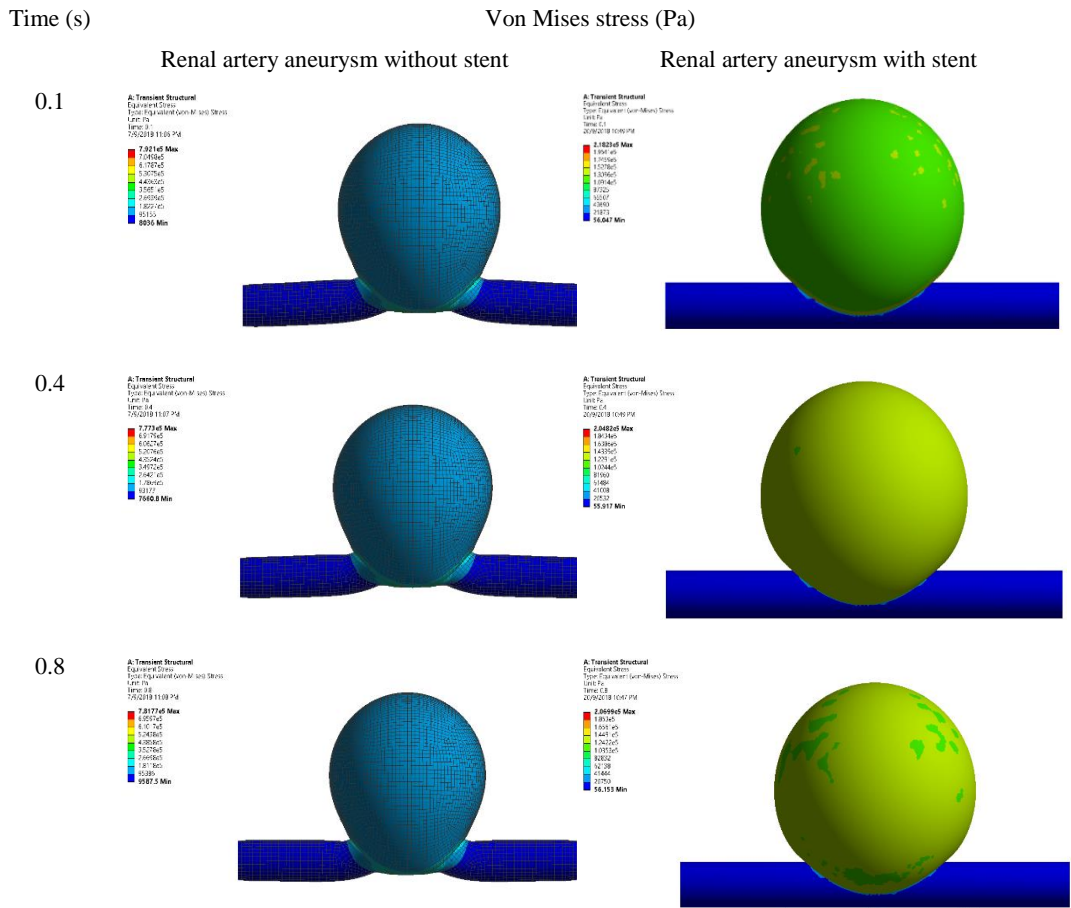


Fig. 12. Von Mises stress for cases of RAA with and without stent.

the RAA without stent exceeds the threshold limit for all the recorded time. This condition, if happens continuously, might lead to the failure of the tissue thus rupturing the aneurysm. With the presence of stent in RAA, the von Mises stress managed to be reduced down to an average of 73.21%, and the stress is lower than the threshold established in this study and other studies as well (Azar *et al.*, 2018; Di Martino *et al.*, 2006; Giannoglou *et al.*, 2006). Hence, the application of stent is of great importance here to protect the tissues from rupture.

4. CONCLUSION

This study is aimed in evaluating the effectiveness of stent based on Abbot RX Herculink type in the treatment of RAA. FSI simulations are conducted to study the hemodynamic of the blood flowing through RAA for the cases of with and without the presence of stent. Flow patterns, WSS, deformation and von Mises stress experienced by RAA are compared and assessed. A simple PIV experiment, observing the flow profile was conducted as a validation steps in ensuring the simulation results are reliable and accurate. The findings show that the simulation and PIV data are in good agreement in terms of the flow profile. The results have also shown that the presence of stent could help in reducing the risk of aneurysm ruptured based on the simulations results obtained.

The stent assisted in reducing the velocity circulation inside the aneurysm dome by 46%. In addition, by obstructing the blood circulating inside the dome, the WSS occurred at the wall of the aneurysm decreased by 71% and the maximum WSS obtained is 0.2182 MPa, which less than the threshold value indication (0.54 MPa) for possible ruptured aneurysm. The stent provided a strong support to the renal artery thereby preventing it from buckling. The von Mises stress declined by 73% when the stent is placed inside the RAA model and successfully protects the RAA from exceeding the threshold limit that may cause rupture.

REFERENCES

Alagheband, M., S. Rahmani, M. Alizadeh, A. Karimi and M. Navidbakhsh (2015). Hemodynamic investigation of intraluminal thrombus effect on the wall stress in a stented three-layered aortic aneurysm model under pulsatile flow. *Artery Research 10* (Supplement C), 11-19.

Antonov, A., K. Kono, K. Greim-Kuczewski, J. E. Hippelheuser, A. Lauric, and A. M. Malek (2018). Proximal Stenosis Is Associated with Rupture Status in Middle Cerebral Artery Aneurysms. *World Neurosurgery*

109, e835-e844.

- Avrahami, I., M. Brand, T. Meirson, Z. Ovadia-Blechman, and M. Halak (2012). Hemodynamic and mechanical aspects of fenestrated endografts for treatment of Abdominal Aortic Aneurysm. *European Journal of Mechanics - B/Fluids* 35, 85-91.
- Azar, D., D. Ohadi, A. Rachev, J. F. Eberth, M. J. Uline and T. Shazly (2018). Mechanical and geometrical determinants of wall stress in abdominal aortic aneurysms: A computational study. *PLOS ONE* 13(2), e0192032.
- Barros, K. J. F., P. B. Metzger F. H., Rossi, T. O. Rodrigues, S. M. Moreira, A. C. G. Petisco and A. M. Kambara (2014). Techniques and Strategies for the Endovascular Treatment of Renal Artery Aneurysm. *Revista Brasileira de Cardiologia Invasiva (English Edition)* 22(1), 64-72.
- Bracale, U. M., D. Narese, I. Ficarelli, M. De Laurentis, F. Spalla, E. Dinoto and F. Pecoraro (2017). Stent-assisted detachable coil embolization of wide-necked renal artery aneurysms. *Diagnostic and Interventional Radiology* 23(1), 77-80.
- Chandra, V., B. W. Ullery and J. T. Lee (2014). Endovascular Stent-Graft Repair of Proximal Renal Artery Aneurysms. *Journal of Vascular Surgery* 60(2), 546-547.
- Chong Ng, F., A. Abas, I. Abustan, Z. Rozainy, M. Z. Abdullah, A. B. Jamaludin, and S. Melissa Kon (2018). *Visualization of Underfill Flow in Ball Grid Array (BGA) using Particle Image Velocimetry (PIV)* (Vol. 370).
- Chrysant, G. S., M. C. Bates, T. M. Sullivan, W. B. Bachinsky, J. J. Popma, L. Peng and M. R. Jaff (2014). Proper patient selection yields significant and sustained reduction in systolic blood pressure following renal artery stenting in patients with uncontrolled hypertension: long-term results from the HERCULES trial. *J Clin Hypertens (Greenwich)* 16(7), 497-503.
- Coleman, D. M. and J. C. Stanley (2015). Renal artery aneurysms. *Journal of Vascular Surgery* 62(3), 779-785.
- Di Martino, E. S., A. Bohra, J. P. Vande Geest, N. Gupta, M. S. Makaroun and D. A. Vorp (2006). Biomechanical properties of ruptured versus electively repaired abdominal aortic aneurysm wall tissue. *Journal of Vascular Surgery* 43(3), 570-576.
- Drewe, C. J., L. P. Parker, L. J. Kelsey, P. E. Norman, J. T. Powell, and B. J. Doyle (2017). Haemodynamics and stresses in abdominal aortic aneurysms: A fluid-structure interaction study into the effect of proximal neck and iliac bifurcation angle. *Journal of Biomechanics* 60(Supplement C), 150-156.
- Du, Y. and V. Lü (2017). Modeling on monitoring the growth and rupture assessment of saccular aneurysms. *Theoretical and Applied Mechanics Letters* 7(2), 117-120.
- Eskandari, M. K. and S. A. Resnick (2005). Aneurysms of the Renal Artery. *Seminars in Vascular Surgery* 18(4), 202-208.
- Giannoglou, G., G. Giannakoulas, J. Soulis, Y. Chatzizisis, T. Perdikides, N. Melas, G. Louridas (2006). Predicting the Risk of Rupture of Abdominal Aortic Aneurysms by Utilizing Various Geometrical Parameters: Revisiting the Diameter Criterion. *Angiology* 57(4), 487-494.
- Hwang, P. F., D. C. Rice, S. V. Patel and D. Mukherjee (2011). Successful management of renal artery aneurysm rupture after cesarean section. *Journal of Vascular Surgery* 54(2), 519-521.
- Javadzadegan, A., B. Fakhim, M. Behnia and M. Behnia (2014). Fluid-structure interaction investigation of spiral flow in a model of abdominal aortic aneurysm. *European Journal of Mechanics - B/Fluids* 46, 109-117.
- Jayendiran, R., B. Nour and A. Ruimi (2018). Fluid-structure interaction (FSI) analysis of stent-graft for aortic endovascular aneurysm repair (EVAR): Material and structural considerations. *Journal of the Mechanical Behavior of Biomedical Materials* 87, 95-110.
- Khe, A. K., A. A. Cherevko, A. P. Chupakhin, M. S. Bobkova, A. L. Krivoschapkin and K. Y. Orlov (2016). Haemodynamics of giant cerebral aneurysm: A comparison between the rigid-wall, one-way and two-way FSI models. *Journal of Physics: Conference Series* 722(1), 012042.
- Klausner, J. Q., P. F. Lawrence, M. P. Harlander-Locke, D. M. Coleman, J. C. Stanley and N. Fujimura (2015). The contemporary management of renal artery aneurysms. *Journal of Vascular Surgery* 61(4), 978-984.e971.
- Leertouwer, T. C., E. J. Gussenhoven, B. C. van Jaarsveld, H. van Overhagen, N. Bom and A. J. Man in 't Veld, (1999). In-vitro validation, with histology, of intravascular ultrasound in renal arteries. *J Hypertens*, 17(2) 271-277.
- Lin, S., X. Han, Y. Bi, S. Ju and L. Gu (2017). Fluid-Structure Interaction in Abdominal Aortic Aneurysm: Effect of Modeling

- Techniques. *BioMed Research International* 10.
- Malacrida, G., I. Dalainas, M. Medda, G. Nano and L. Inglese (2007). Endovascular Treatment of a Renal Artery Branch Aneurysm. *CardioVascular and Interventional Radiology* 30(1), 118-120.
- Maughan, E., C. Webster, T. Konig and I. Renfrew (2015). Endovascular management of renal artery aneurysm rupture in pregnancy – A case report. *International Journal of Surgery Case Reports* 12, 41-43.
- Mokhtar, N. H., A. Abas, N. A.Razak, M. N. A. Hamid and S. L.Teong (2017). Effect of different stent configurations using Lattice Boltzmann method and particles image velocimetry on artery bifurcation aneurysm problem *Journal of Theoretical Biology* 433(supplimen C) 73-84
- Mulder, G., A. C. B. Bogaerds, P. Rongen and F. N. van de Vosse (2009). On automated analysis of flow patterns in cerebral aneurysms based on vortex identification. *Journal of Engineering Mathematics* 64(4), 391.
- Muzaffer D., F. Bayrak, B. Mutlu, B. Gürses, S. Güran and E. Demirtas (2006). Large Renal Artery Aneurysm Treated With Stent Graft. *Circulation* 113(23), e848–e849.
- Myer, K. (2003). *Physical And Flow Properties of Blood*, Standard Handbook of Biomedical Engineering & Design: McGraw Hill Professional, Access Engineering.
- Rissland, P., Y. Alemu, S. Einav, J. Ricotta and D. Bluestein (2009). Abdominal aortic aneurysm risk of rupture: patient-specific FSI simulations using anisotropic model. *J Biomech Eng* 131(3), 031001.
- Sahin, S., M. Okbay, B. Cinar and N. Uzunlulu (2007). Wide-necked renal artery aneurysm: endovascular treatment with stent-graft. *Diagn Interv Radiol* 13(1), 42-45.
- Sharzehee, M., S. S. Khalafvand and H. C. Han (2018). Fluid-structure interaction modeling of aneurysmal arteries under steady-state and pulsatile blood flow: a stability analysis. *Computer Methods in Biomechanics and Biomedical Engineering* 21(3), 219-231.
- Sinnott, M., P. Cleary and M. Prakash (2006). *An investigation of pulsatile blood flow in a bifurcation artery using a grid-free method*. Paper presented at the Fifth international conference on CFD in the process industries Melbourne, Australia
- Sousa, J. and A. Mansilha (2017). Endovascular Treatment of Symptomatic Renal Artery Aneurysm with Hostile Anatomy. *Eur J Vasc Endovasc Surg* 53(6), 843.
- Suess, T., J. Anderson, L. Danielson, K. Pohlson, T. Remund, E. Blears and P. Kelly (2016). Examination of near-wall hemodynamic parameters in the renal bridging stent of various stent graft configurations for repairing visceral branched aortic aneurysms. *Journal of Vascular Surgery* 64(3), 788-796.
- Tsilimparis, N., J. G. Reeves, A. Dayama, S. D. Perez, E. S. Debus and J. J. Ricotta (2013). Endovascular vs Open Repair of Renal Artery Aneurysms: Outcomes of Repair and Long-Term Renal Function. *Journal of the American College of Surgeons* 217(2), 263-269.
- Valencia, A., P. Burdiles, M. Ignat, J. Mura, E. Bravo, R. Rivera and J. Sordo (2013). Fluid Structural Analysis of Human Cerebral Aneurysm Using Their Own Wall Mechanical Properties. *Computational and Mathematical Methods in Medicine*, 293128.
- Varble, N., G. Trylesinski, J. Xiang, K. Snyder and H. Meng (2017). Identification of vortex structures in a cohort of 204 intracranial aneurysms. *Journal of The Royal Society Interface* 14(130).
- Wang, X. and X. Li (2011). Computational simulation of aortic aneurysm using FSI method: Influence of blood viscosity on aneurysmal dynamic behaviors. *Computers in Biology and Medicine* 41(9), 812-821.
- Wang, Y., S. Song, G. Zhou, D. Liu, X. Xia, B., Liang and G. Feng, (2018). Strategy of endovascular treatment for renal artery aneurysms. *Clinical Radiology* 73(4), 414.e411-414.e415.
- Yeow, S. L. and H. L. Leo (2016). *Hemodynamic Study of Flow Remodeling Stent Graft for the Treatment of Highly Angulated Abdominal Aortic Aneurysm* (Vol. 2016).
- Yeow, S. L. and H. L. Leo (2016). Hemodynamic Study of Flow Remodeling Stent Graft for the Treatment of Highly Angulated Abdominal Aortic Aneurysm. *Computational and Mathematical Methods in Medicine*, 3830123.
- Yiemeng H., H. Meng, H. Scott Woodward, Bernard R. Bendok, Ricardo A. Hanel, Lee R. Guterman, & L. Nelson Hopkins. (2004). Effects of arterial geometry on aneurysm growth: three-dimensional computational fluid dynamics study. *Journal of Neurosurgery* 101(4), 676-681.

